

Excited-State Effects on Magnetic Properties of U(III) and U(IV) Pyrazolylborate Complexes.

Robert F. Higgins,[†] Caleb J. Tatebe,[‡] Suzanne C. Bart,[‡] Matthew P. Shores^{†*}

[†]Department of Chemistry, Colorado State University, Fort Collins, Colorado 80523, United States

[‡]H. C. Brown Laboratory, Department of Chemistry, Purdue University, West Lafayette, Indiana 47906, United States

Email: matthew.shores@colostate.edu

Table of Contents

Preparation of compounds	3
Magnetic properties	3
Figure S1. Field dependence of magnetization for compound [Tp* ₂ U]-insert collected at 100 K. The data are fit to a linear regression ($y = 0.0121x - 4.21E-4$) that does not include $H = 0$ Oe.	5
Figure S2. Field dependence of magnetization for compound [Tp* ₂ U(THF)](BPh ₄) collected at 100 K. The data are fit to a linear regression ($y = 0.0227x - 5.37E-4$) that does not include $H = 0$ Oe.	6
Figure S3. Field dependence of magnetization for compound [Tp* ₂ U(MeCN) ₂](BPh ₄) collected at 100 K. The data are fit to a linear regression ($y = 0.0144x - 1.10E-4$) that does not include $H = 0$ Oe.	6
Figure S4. Temperature dependence of the magnetic susceptibility for [Tp* ₂ U]-insert collected at 1000 Oe.	7
Figure S5. Temperature dependence of the magnetic susceptibility for two different batches of compound [Tp* ₂ U(THF)](BPh ₄), both collected at 5000 Oe.	7
Figure S6. Temperature dependence of the magnetic susceptibility for two different batches of compound [Tp* ₂ U(MeCN) ₂](BPh ₄), both collected at 1000 Oe.	7
Figure S7. Field dependence of magnetization for [Tp* ₂ U]-amidinate collected at 1.8 K.	8
Figure S8. Field dependence of magnetization for [Tp* ₂ U(THF)](BPh ₄) collected at 1.8 K.	8
Figure S9. Field dependence of magnetization for [Tp* ₂ U(MeCN) ₂](BPh ₄) collected at 1.8 K.	9
Figure S10. Temperature dependence of the magnetic susceptibility for compounds [(Tp* ₂ U) ₂ - <i>p</i> -DEB], [(Tp* ₂ U) ₂ - <i>m</i> -DEB], [Tp* ₂ UCCPh], [Tp* ₂ U(THF)](BPh ₄) and [Tp* ₂ U(MeCN) ₂](BPh ₄) collected at 1000, 1000, 5000, 5000 and 1000 Oe, respectively. The lines correspond to the best fits obtained using the program PHI. ⁴	9
Figure S11. Temperature dependence of the magnetic susceptibility for [Tp* ₂ U(bpy)]I. Data were digitized from a previous report. ⁵ The line corresponds to the best fits obtained using the program PHI. ⁴	9
Figure S12. Temperature dependence of the magnetic susceptibility for [Tp* ₂ UI]. Data were digitized from a previous report. ⁶ The line corresponds to the best fits obtained using the program PHI. ⁴	10
Figure S13. Temperature dependence of the magnetic susceptibility for [U(BPz ₂ H ₂) ₃]. Data were digitized from a previous report. ⁷ The line corresponds to the best fits obtained using the program PHI. ⁴	10
Figure S14. Field and frequency dependence of the in-phase magnetic susceptibility for compound [(Tp* ₂ U) ₂ - <i>p</i> -DEB] collected at 2 K (4 Oe ac field).	11

Figure S15. Field and frequency dependence of the out-of-phase magnetic susceptibility for compound [(Tp* ₂ U) ₂ - <i>p</i> -DEB] collected at 2 K (4 Oe ac field).	11
Figure S16. Field and frequency dependence of the in-phase magnetic susceptibility for compound [(Tp* ₂ U) ₂ - <i>m</i> -DEB] collected at 2 K (4 Oe ac field).	12
Figure S17. Field and frequency dependence of the out-of-phase magnetic susceptibility for compound [(Tp* ₂ U) ₂ - <i>m</i> -DEB] collected at 2 K (4 Oe ac field).	12
Figure S18. Field dependence of the in-phase magnetic susceptibility for [Tp* ₂ UCCPh] collected with an applied ac field of 4 Oe at 1.8 K.	13
Figure S19. Field dependence of the out-of-phase magnetic susceptibility for [Tp* ₂ UCCPh] collected with an applied ac field of 4 Oe at 1.8 K.	13
Figure S20. Temperature dependence of the in-phase magnetic susceptibility for [Tp* ₂ UCCPh] collected with an applied ac field of 4 Oe and an applied dc field of 1000 Oe.	14
Figure S21. Temperature dependence of the out-of-phase magnetic susceptibility for [Tp* ₂ UCCPh] collected with an applied ac field of 4 Oe and an applied dc field of 1000 Oe.	14
Figure S22. Field dependence of the in-phase magnetic susceptibility for [Tp* ₂ U(THF)](BPh ₄) collected with an applied ac field of 4 Oe at 1.8 K.	14
Figure S23. Field dependence of the out-of-phase magnetic susceptibility for [Tp* ₂ U(THF)](BPh ₄) collected with an applied ac field of 4 Oe at 1.8 K.	15
Figure S24. Temperature dependence of the in-phase magnetic susceptibility for [Tp* ₂ U(THF)](BPh ₄) collected with an applied ac field of 4 Oe and an applied dc field of 500 Oe.	15
Figure S25. Temperature dependence of the out-of-phase magnetic susceptibility for [Tp* ₂ U(THF)](BPh ₄) collected with an applied ac field of 4 Oe and an applied dc field of 500 Oe.	16
Figure S26. Field dependence of the in-phase magnetic susceptibility for [Tp* ₂ U(MeCN) ₂](BPh ₄) collected with an applied ac field of 4 Oe at 1.8 K.	16
Figure S27. Field dependence of the out-of-phase magnetic susceptibility for [Tp* ₂ U(MeCN) ₂](BPh ₄) collected with an applied ac field of 4 Oe at 1.8 K.	16
Figure S28. Arrhenius plot using peak maxima data from the out-of-phase magnetic susceptibility for [Tp* ₂ UCCPh], [Tp* ₂ U(THF)](BPh ₄) and [Tp* ₂ U(MeCN) ₂](BPh ₄).	17
Figure S29. Fits of the peak maxima data from the out-of-phase magnetic susceptibility to a Raman function ($\tau^{-1} = CT^n$) for [Tp* ₂ UCCPh], [Tp* ₂ U(THF)](BPh ₄) and [Tp* ₂ U(MeCN) ₂](BPh ₄), where <i>C</i> and <i>n</i> are the Raman coefficient and exponent, respectively.	18
Figure S30. Temperature dependence of the magnetic susceptibility for [(Tp* ₂ U) ₂ - <i>p</i> -DIB] collected at 1000 Oe with associated PHI fit. Note: susceptibility is shown per U ion.	18
Figure S31. Inverse temperature dependence of the magnetic susceptibility for [(Tp* ₂ U) ₂ - <i>p</i> -DIB] collected at 1000 Oe with associated PHI fit. Note: susceptibility is shown per U ion.	18
Figure S32. Temperature dependence of the magnetic susceptibility for [(Tp* ₂ U) ₂ - <i>p</i> -DIB] collected at 1000 Oe with associated PHI fit. Note: susceptibility is shown per U ion.	19
Figure S33. Temperature dependence of the magnetic susceptibility for [(Tp* ₂ U) ₂ - <i>p</i> -DIB] collected at 1000 Oe with associated PHI fit. Note: susceptibility is shown per U ion.	19

Figure S34. Temperature dependence of the magnetic susceptibility for [(Tp* ₂ U) ₂ - <i>m</i> -DIB] collected at 1000 Oe with associated PHI fit. Note: susceptibility is shown per U ion.	20
Figure S35. Inverse temperature dependence of the magnetic susceptibility for [(Tp* ₂ U) ₂ - <i>m</i> -DIB] collected at 1000 Oe with associated PHI fit. Note: susceptibility is shown per U ion.	20
Figure S36. Temperature dependence of the magnetic susceptibility for [(Tp* ₂ U) ₂ - <i>m</i> -DIB] collected at 1000 Oe with associated PHI fit. Note: susceptibility is shown per U ion.	20
Figure S37. Temperature dependence of the magnetic susceptibility for [(Tp* ₂ U) ₂ - <i>m</i> -DIB] collected at 1000 Oe with associated PHI fit. Note: susceptibility is shown per U ion.	21
Figure S38. Temperature dependence of the magnetic susceptibility for [Tp* ₂ U=N- <i>p</i> -Tol] collected at 5000 Oe with associated PHI fit.	21
Figure S39. Inverse temperature dependence of the magnetic susceptibility for [Tp* ₂ U=N- <i>p</i> -Tol] collected at 5000 Oe with associated PHI fit.	22
Figure S40. Temperature dependence of the magnetic susceptibility for [Tp* ₂ U=N- <i>p</i> -Tol] collected at 5000 Oe with associated PHI fit.	22
Figure S41. Temperature dependence of the magnetic susceptibility for [Tp* ₂ U=N- <i>p</i> -Tol] collected at 5000 Oe with associated PHI fit.	23
Figure S42. Temperature dependence of the magnetic susceptibility for [Tp* ₂ U]-amidinate collected at 1000 Oe with associated PHI fit.	23
Figure S43. Inverse temperature dependence of the magnetic susceptibility for [Tp* ₂ U]-amidinate collected at 1000 Oe with associated PHI fit.	24
Figure S44. Temperature dependence of the magnetic susceptibility for [Tp* ₂ U]-amidinate collected at 1000 Oe with associated PHI fit.	24
Figure S45. Temperature dependence of the magnetic susceptibility for [Tp* ₂ U]-amidinate collected at 1000 Oe with associated PHI fit.	25
Table S1. Selected crystallographic parameters for U(Tp*) complexes.	25
Table S2. Comparison of different magnetic and crystallographic properties of U(Tp*) complexes.	25
References	25

Preparation of compounds

All compounds were prepared by the methods described in previous reports.^{1,2}

Magnetic properties

Magnetic susceptibility data were collected using a Quantum Design MPMS XL SQUID magnetometer.

All sample preparations were performed inside a dinitrogen-filled glovebox (MBRAUN Labmaster 130).

Powdered microcrystalline samples were loaded into polyethylene bags and sealed in the glovebox. The

bags that contained compounds $[\text{Tp}^*_2\text{U}(\text{MeCN})_2](\text{BPh}_4)$ and $[\text{Tp}^*_2\text{U}(\text{THF})](\text{BPh}_4)$ were subsequently sealed in an additional polyethylene bag to ensure inert conditions as these complexes showed heightened air-sensitivity. After sealing in the bags, the samples were inserted into a straw and transported to the magnetometer under dinitrogen. Ferromagnetic impurities were checked through a variable field analysis (0 to 10 kOe) of the magnetization at 100 K (Figures S1-S3), which showed that for $[\text{Tp}^*_2\text{U}(\text{MeCN})_2](\text{BPh}_4)$ and the insertion product major ferromagnetic impurities were likely not present. As a precaution, the variable temperature magnetic susceptibility data for $[\text{Tp}^*_2\text{U}(\text{THF})](\text{BPh}_4)$ were collected at 5000 Oe due to non-linearity in the magnetization data collected at 100 K. Magnetic susceptibility data were collected at temperatures ranging from 2 to 300 K (Figure S4-S6). Reproducibility of magnetic susceptibility data was assessed through measurements on two different batches for all compounds measured, which showed relative consistency at all temperatures (Figures S4-S6). Magnetization measurements were collected at 1.8 K while varying the applied field up to 50 kOe (Figures S7-S9). Dynamic magnetic measurements were performed with a 4 Oe applied ac field (Figure S14-S27). Fits that include crystal field and magnetic anisotropic parameters used the following equation:

$$\hat{H} = \sum D_i [S_{z,i}^2 - 1/3 S_i(S_i + 1) + E_i/D_i (S_{x,i}^2 - S_{y,i}^2)] + \sum g_{xx,i} \beta \hat{S}_{x,i} \cdot \hat{B}_x + g_{yy,i} \beta \hat{S}_{y,i} \cdot \hat{B}_y + g_{zz,i} \beta \hat{S}_{z,i} \cdot \hat{B}_z + \sum_{k=2,4,6}^k \sum_{q=-k}^k B_k^q \hat{O}_k^q + \mu_B g_j \hat{J} \cdot \hat{B}$$

Fits that include only crystal field parameters used the following equation:

$$\hat{H} = \sum_{k=2,4,6}^k \sum_{q=-k}^k B_k^q \hat{O}_k^q + \mu_B g_j \hat{J} \cdot \hat{B}$$

Where D = axial anisotropy, E = rhombic anisotropy, S = spin state, B^0_2 = axial crystal field parameter, \hat{O}^0 = Stevens operators, μ_B = Bohr magneton, J = exchange coupling parameter, g_j = Lande factor and \hat{B} = magnetic field. Data were corrected for the diamagnetic contributions of the sample holder and bag by subtracting empty containers; corrections for the sample were calculated from Pascal's constants.³

Further description for some of the fits

When an $S = 1$ impurity is included in the fits for compounds $[\text{Tp}^*_2\text{U}=\text{N}-p\text{-Tol}]$, $[(\text{Tp}^*_2\text{U})_2-p\text{-DIB}]$ and $[(\text{Tp}^*_2\text{U})_2-m\text{-DIB}]$, the quality of the fit did not greatly improve, and the impurity consistently remained

below 0.01%, indicative that these compounds are free of paramagnetic impurities. Further, if these fits are performed using two distinct U ions for $[(\text{Tp}^*_2\text{U})_2\text{-}p\text{-DIB}]$ and $[(\text{Tp}^*_2\text{U})_2\text{-}m\text{-DIB}]$, no reasonable fits are obtained. For the U(III) complexes, the same crystal field parameters were included in the Hamiltonian and the inclusion of an axial anisotropy term, D , to compare with previously reported calculations on $[\text{Tp}^*_2\text{U}]^+$ fragments.⁶ The rhombic anisotropy term, E , was held at zero to avoid any potential overparameterization, considering that 4 parameters were used in the fit. When fits were performed on the U(III) complexes with only the inclusion of either the term D or B^0_2 , the low temperature regime did not fit well. Therefore both were required to accurately model the data.

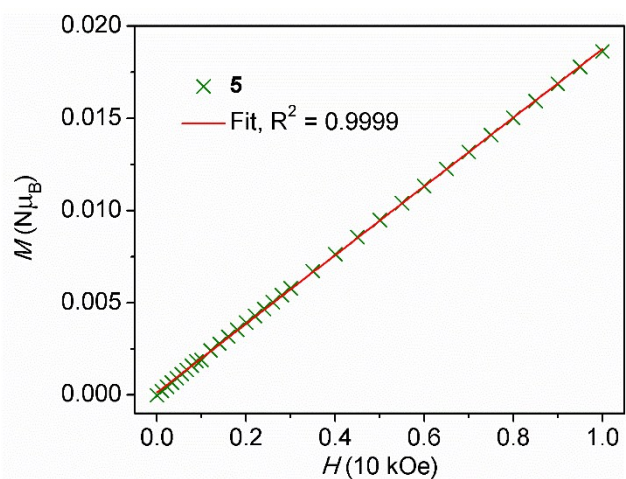


Figure S1. Field dependence of magnetization for compound $[\text{Tp}^*_2\text{U}]$ -insert collected at 100 K. The data are fit to a linear regression ($y = 0.0121x - 4.21\text{E-}4$) that does not include $H = 0$ Oe.

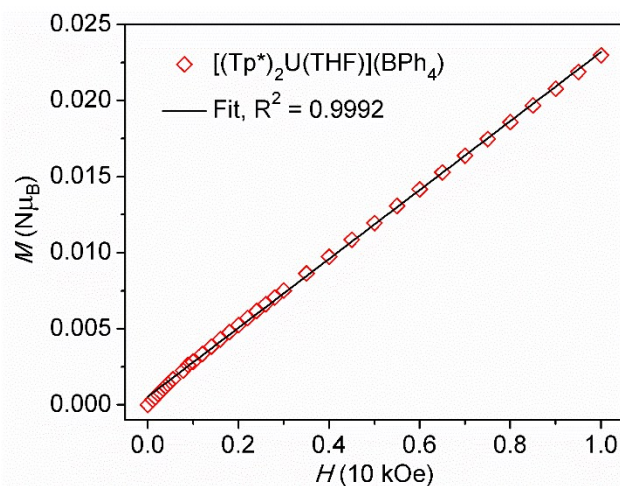


Figure S2. Field dependence of magnetization for compound $[\text{Tp}^*_2\text{U}(\text{THF})](\text{BPh}_4)$ collected at 100 K. The data are fit to a linear regression ($y = 0.0227x - 5.37\text{E-}4$) that does not include $H = 0$ Oe.

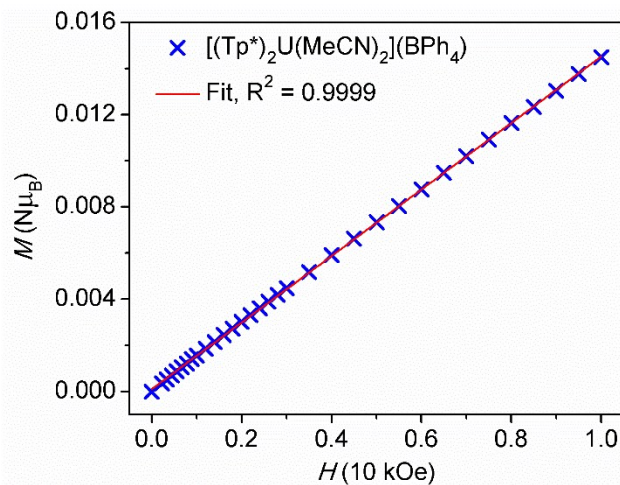


Figure S3. Field dependence of magnetization for compound $[\text{Tp}^*_2\text{U}(\text{MeCN})_2](\text{BPh}_4)$ collected at 100 K. The data are fit to a linear regression ($y = 0.0144x - 1.10\text{E-}4$) that does not include $H = 0$ Oe.

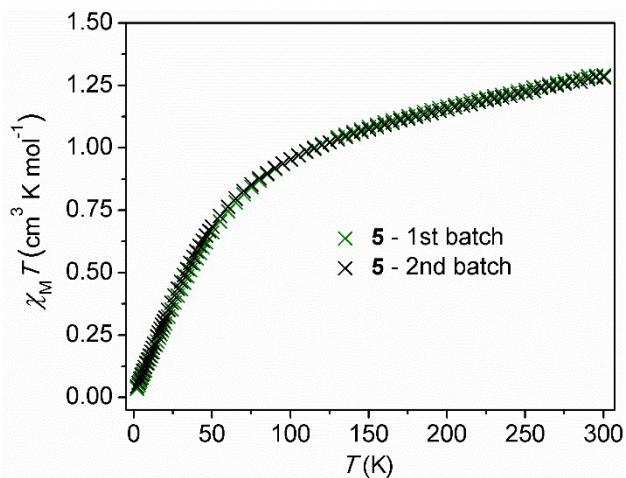


Figure S4. Temperature dependence of the magnetic susceptibility for $[\text{Tp}^*_2\text{U}]$ -insert collected at 1000 Oe.

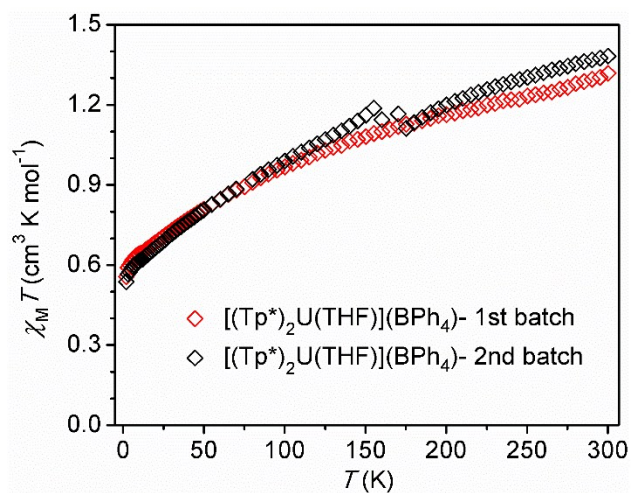


Figure S5. Temperature dependence of the magnetic susceptibility for two different batches of compound $[\text{Tp}^*_2\text{U}(\text{THF})](\text{BPh}_4)$, both collected at 5000 Oe.

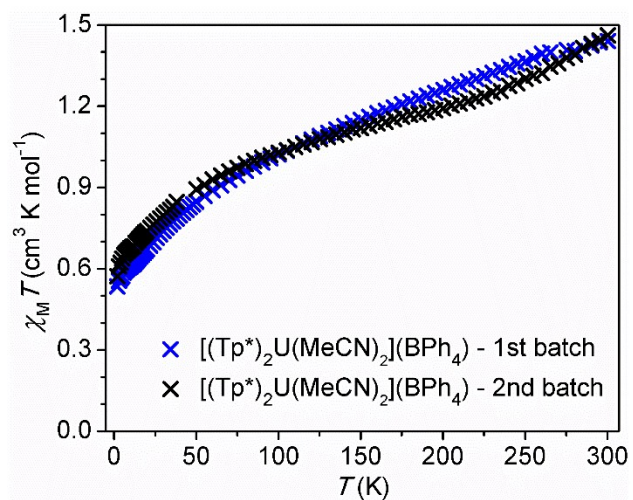


Figure S6. Temperature dependence of the magnetic susceptibility for two different batches of compound $[\text{Tp}^*_2\text{U}(\text{MeCN})_2](\text{BPh}_4)$, both collected at 1000 Oe.

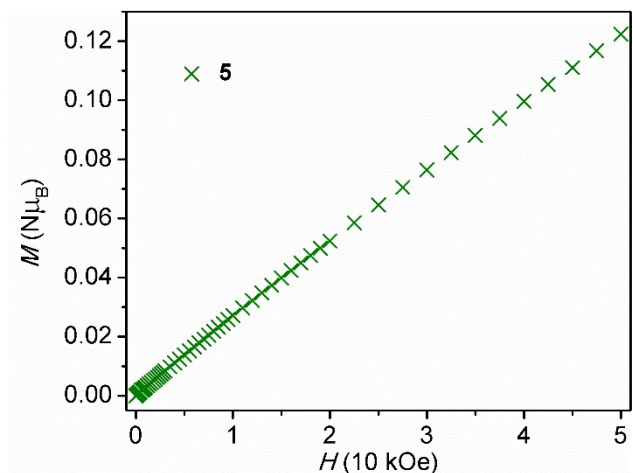


Figure S7. Field dependence of magnetization for $[\text{Tp}^*_2\text{U}]$ -amidinate collected at 1.8 K.

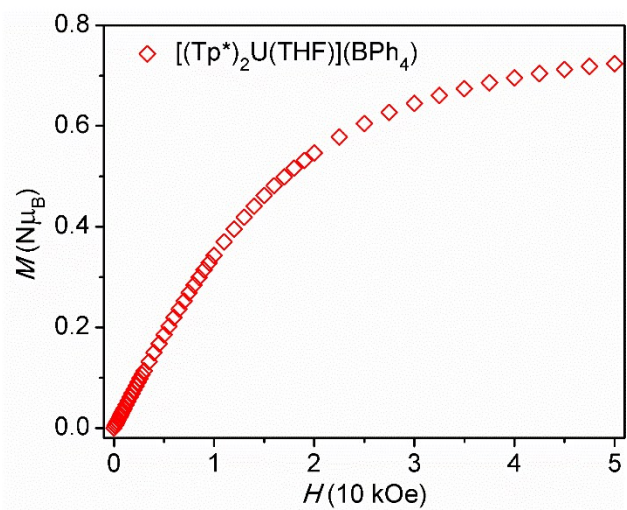


Figure S8. Field dependence of magnetization for $[\text{Tp}^*_2\text{U}(\text{THF})](\text{BPh}_4)$ collected at 1.8 K.

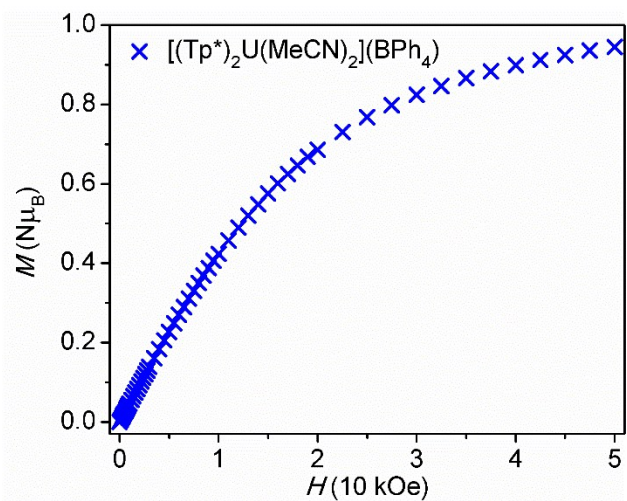


Figure S9. Field dependence of magnetization for $[\text{Tp}^*_2\text{U}(\text{MeCN})_2](\text{BPh}_4)$ collected at 1.8 K.

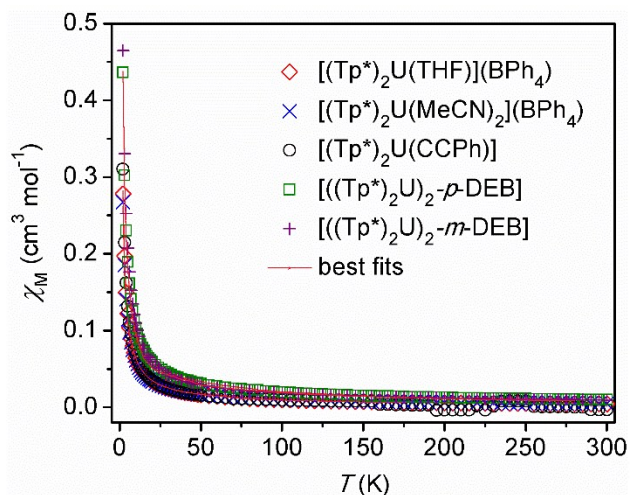


Figure S10. Temperature dependence of the magnetic susceptibility for compounds $[(\text{Tp}^*_2\text{U})_2\text{-}p\text{-DEB}]$, $[(\text{Tp}^*_2\text{U})_2\text{-}m\text{-DEB}]$, $[\text{Tp}^*_2\text{UCCPh}]$, $[\text{Tp}^*_2\text{U}(\text{THF})](\text{BPh}_4)$ and $[\text{Tp}^*_2\text{U}(\text{MeCN})_2](\text{BPh}_4)$ collected at 1000, 1000, 5000, 5000 and 1000 Oe, respectively. The lines correspond to the best fits obtained using the program PHI.⁴

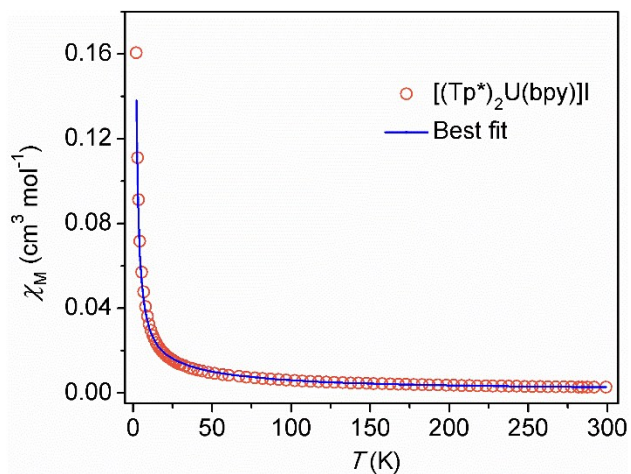


Figure S11. Temperature dependence of the magnetic susceptibility for $[\text{Tp}^*_2\text{U}(\text{bpy})]\text{I}$. Data were digitized from a previous report.⁵ The line corresponds to the best fits obtained using the program PHI.⁴

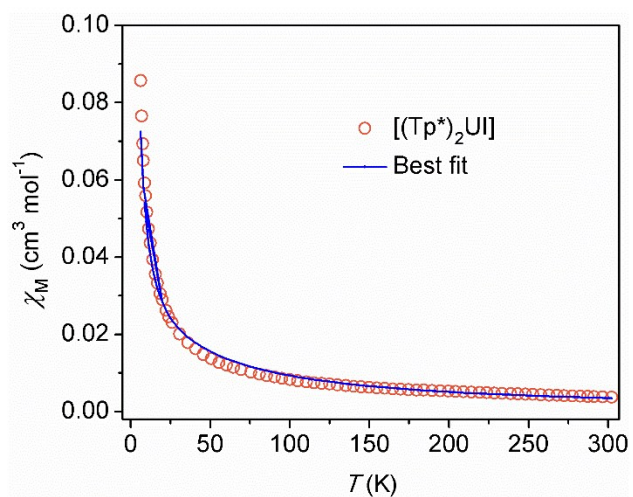


Figure S12. Temperature dependence of the magnetic susceptibility for $[(Tp^*)_2U]$. Data were digitized from a previous report.⁶ The line corresponds to the best fits obtained using the program PHI.⁴

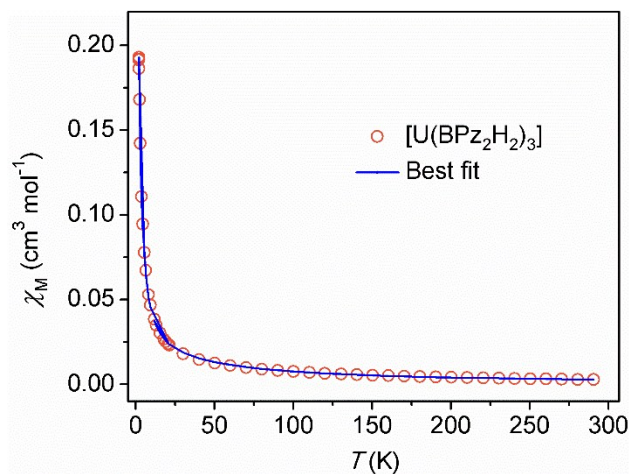


Figure S13. Temperature dependence of the magnetic susceptibility for $[U(BPz_2H_2)_3]$. Data were digitized from a previous report.⁷ The line corresponds to the best fits obtained using the program PHI.⁴

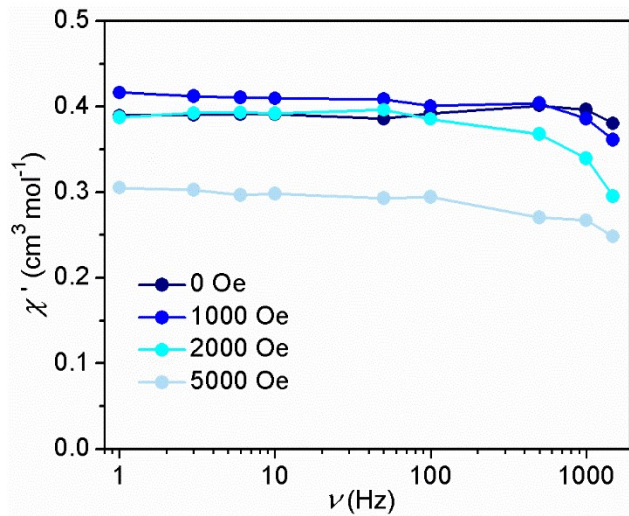


Figure S14. Field and frequency dependence of the in-phase magnetic susceptibility for compound $[(\text{Tp}^*\text{U})_2\text{-}p\text{-DEB}]$ collected at 2 K (4 Oe ac field).

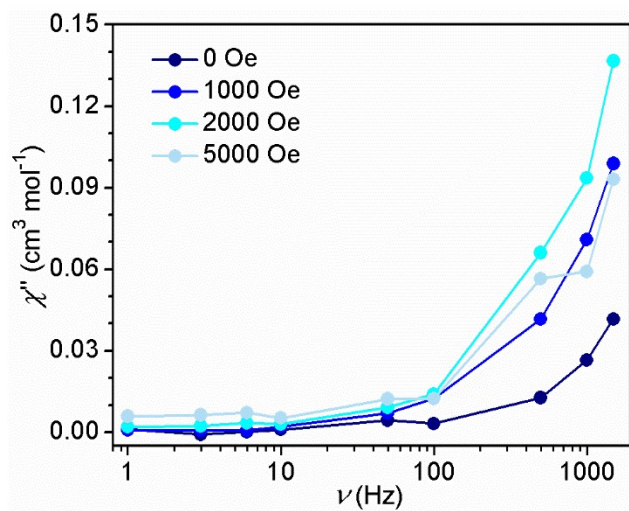


Figure S15. Field and frequency dependence of the out-of-phase magnetic susceptibility for compound $[(\text{Tp}^*\text{U})_2\text{-}p\text{-DEB}]$ collected at 2 K (4 Oe ac field).

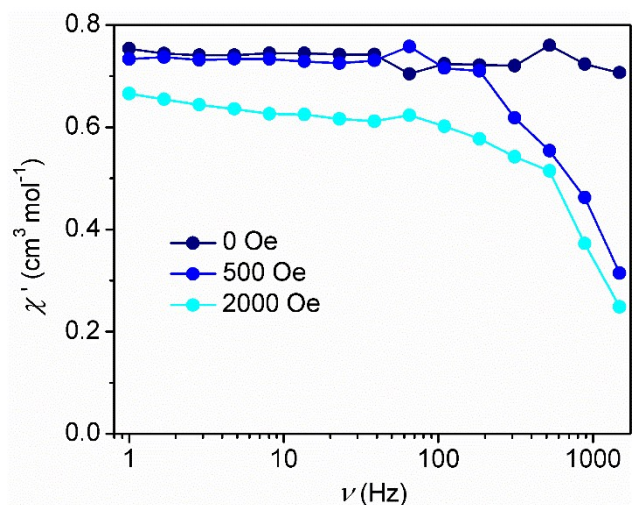


Figure S16. Field and frequency dependence of the in-phase magnetic susceptibility for compound [(Tp*₂U)₂-m-DEB] collected at 2 K (4 Oe ac field).

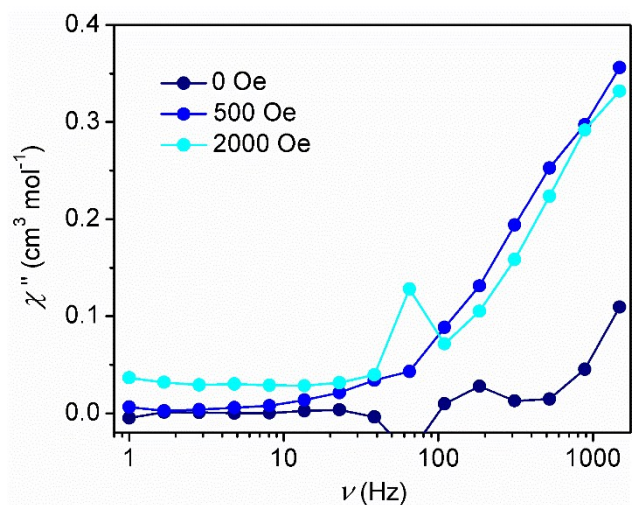


Figure S17. Field and frequency dependence of the out-of-phase magnetic susceptibility for compound [(Tp*₂U)₂-m-DEB] collected at 2 K (4 Oe ac field).

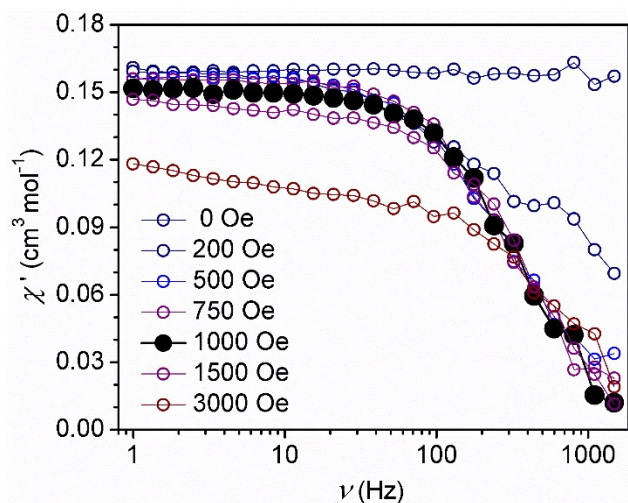


Figure S18. Field dependence of the in-phase magnetic susceptibility for $[\text{Tp}^*_2\text{UCCPh}]$ collected with an applied ac field of 4 Oe at 1.8 K.

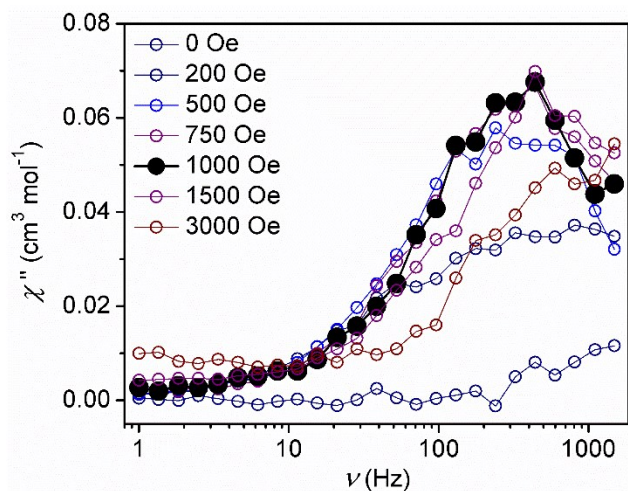


Figure S19. Field dependence of the out-of-phase magnetic susceptibility for $[\text{Tp}^*_2\text{UCCPh}]$ collected with an applied ac field of 4 Oe at 1.8 K.

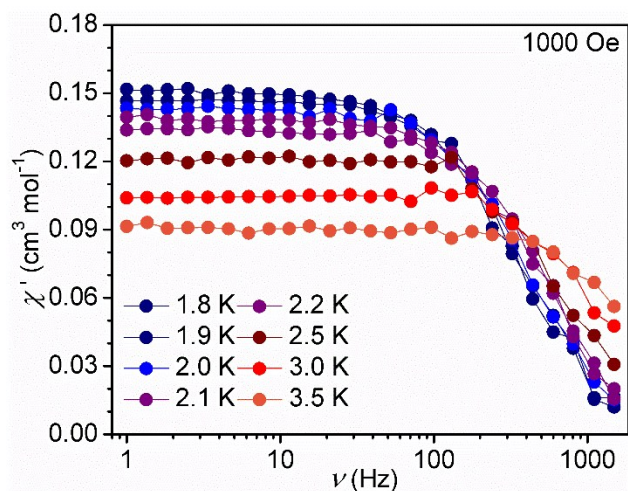


Figure S20. Temperature dependence of the in-phase magnetic susceptibility for [Tp*₂UCCPh] collected with an applied ac field of 4 Oe and an applied dc field of 1000 Oe.

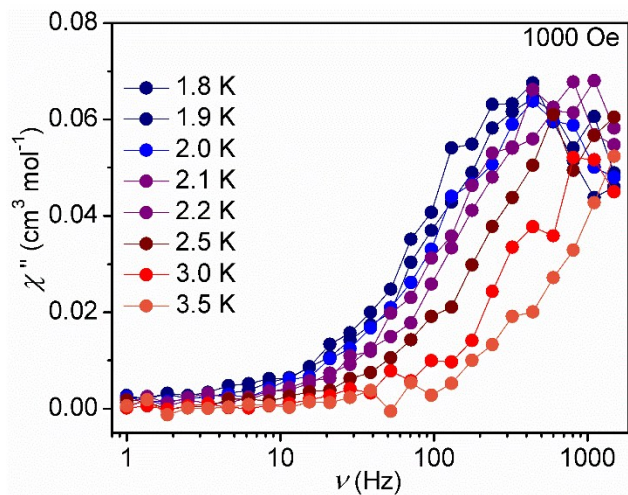


Figure S21. Temperature dependence of the out-of-phase magnetic susceptibility for [Tp*₂UCCPh] collected with an applied ac field of 4 Oe and an applied dc field of 1000 Oe.

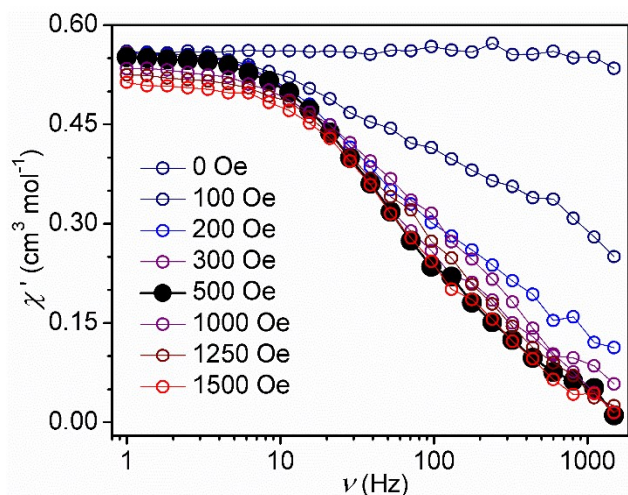


Figure S22. Field dependence of the in-phase magnetic susceptibility for [Tp*₂U(THF)](BPh₄) collected with an applied ac field of 4 Oe at 1.8 K.

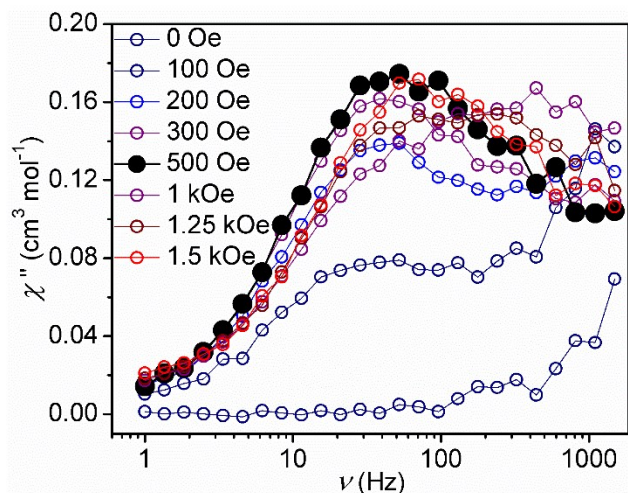


Figure S23. Field dependence of the out-of-phase magnetic susceptibility for $[\text{Tp}^*_2\text{U}(\text{THF})](\text{BPh}_4)$ collected with an applied ac field of 4 Oe at 1.8 K.

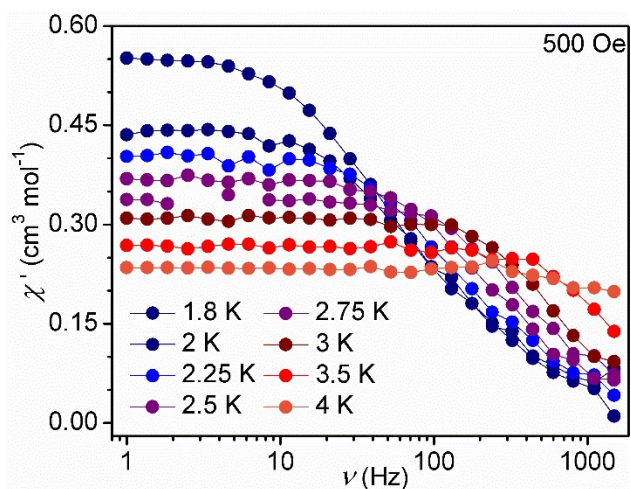


Figure S24. Temperature dependence of the in-phase magnetic susceptibility for $[\text{Tp}^*_2\text{U}(\text{THF})](\text{BPh}_4)$ collected with an applied ac field of 4 Oe and an applied dc field of 500 Oe.

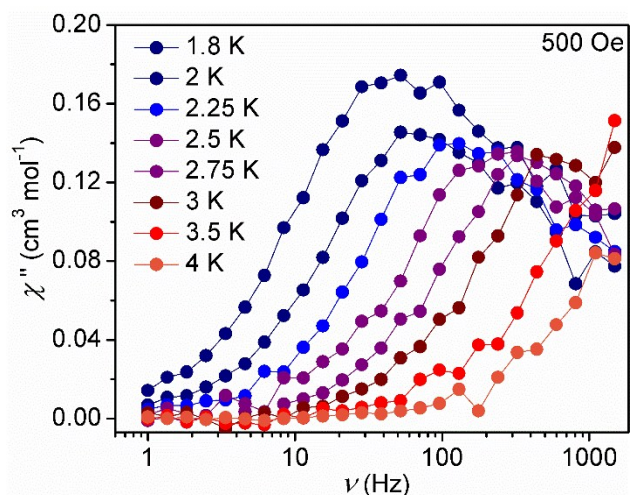


Figure S25. Temperature dependence of the out-of-phase magnetic susceptibility for $[\text{Tp}^*_2\text{U}(\text{THF})](\text{BPh}_4)$ collected with an applied ac field of 4 Oe and an applied dc field of 500 Oe.

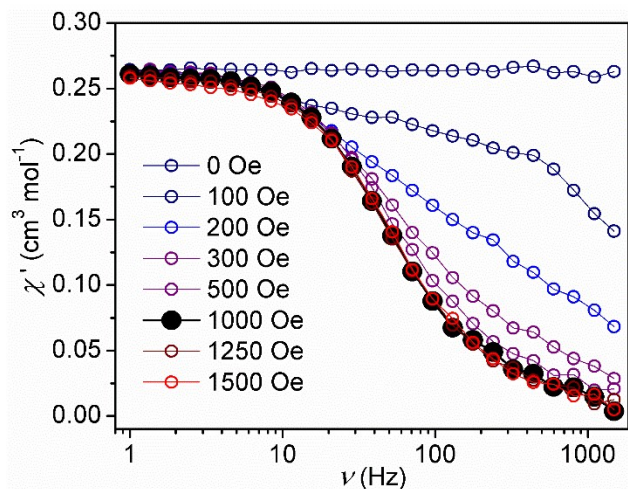


Figure S26. Field dependence of the in-phase magnetic susceptibility for $[\text{Tp}^*_2\text{U}(\text{MeCN})_2](\text{BPh}_4)$ collected with an applied ac field of 4 Oe at 1.8 K.

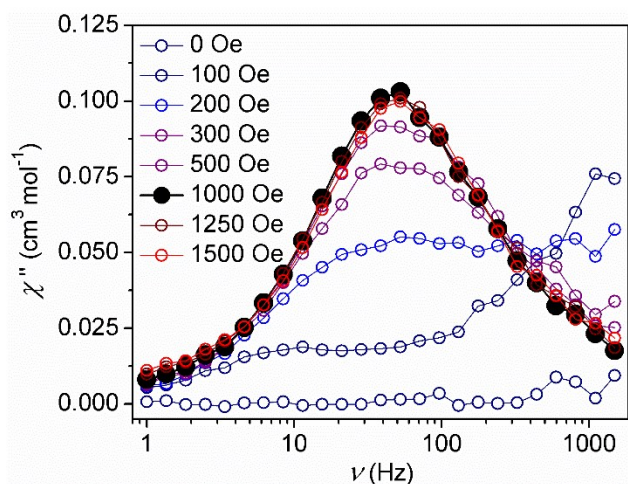


Figure S27. Field dependence of the out-of-phase magnetic susceptibility for $[\text{Tp}^*_2\text{U}(\text{MeCN})_2](\text{BPh}_4)$ collected with an applied ac field of 4 Oe at 1.8 K.

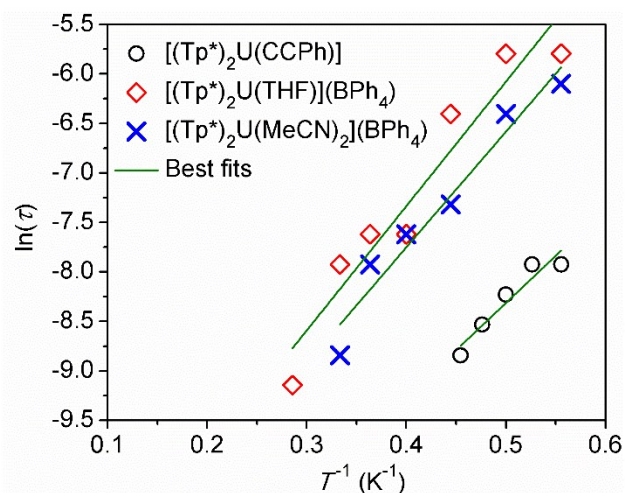


Figure S28. Arrhenius plot using peak maxima data from the out-of-phase magnetic susceptibility for $[Tp^*_2UCCPh]$, $[Tp^*_2U(THF)](BPh_4)$ and $[Tp^*_2U(MeCN)_2](BPh_4)$.

The data in Figure S28 indicate that the primary relaxation pathway for all of these complexes occurs through Raman relaxation; however, at high temperature, there are Orbach contributions observable through the more linear behavior. All of the data were fit to remain consistent with literature precedent. The Orbach contribution is further supported by the larger τ_0 values that were determined for $[Tp^*_2UCCPh]$, $[Tp^*_2U(THF)](BPh_4)$ and $[Tp^*_2U(MeCN)_2](BPh_4)$ compared to other $[Tp^*_2U]^+$ complexes.^{5,6}

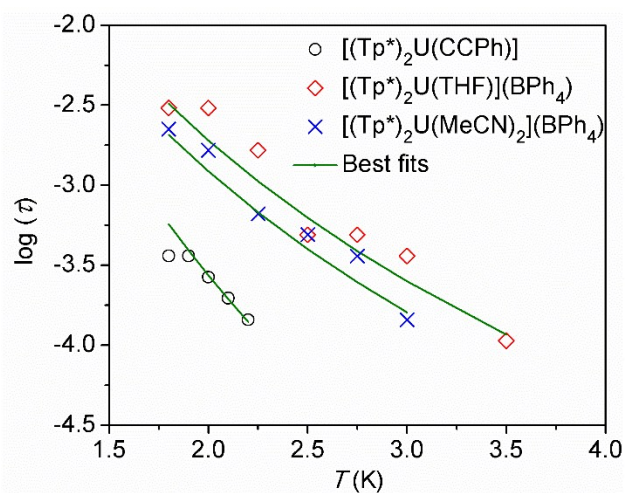


Figure S29. Fits of the peak maxima data from the out-of-phase magnetic susceptibility to a Raman function ($\tau^{-1} = CT^n$) for $[\text{Tp}^*_2\text{UCCPh}]$, $[\text{Tp}^*_2\text{U}(\text{THF})](\text{BPh}_4)$ and $[\text{Tp}^*_2\text{U}(\text{MeCN})_2](\text{BPh}_4)$, where C and n are the Raman coefficient and exponent, respectively.

The values obtained for the fits were as follows: $C = 0.035$, $n = 7$ for $[\text{Tp}^*_2\text{UCCPh}]$; $C = 0.069$, $n = 5$ for $[\text{Tp}^*_2\text{U}(\text{THF})](\text{BPh}_4)$; $C = 0.039$, $n = 5$ for $[\text{Tp}^*_2\text{U}(\text{MeCN})_2](\text{BPh}_4)$. Note: The lowest temperature (1.8 K) data point for $[\text{Tp}^*_2\text{UCCPh}]$ was not included for these fits.

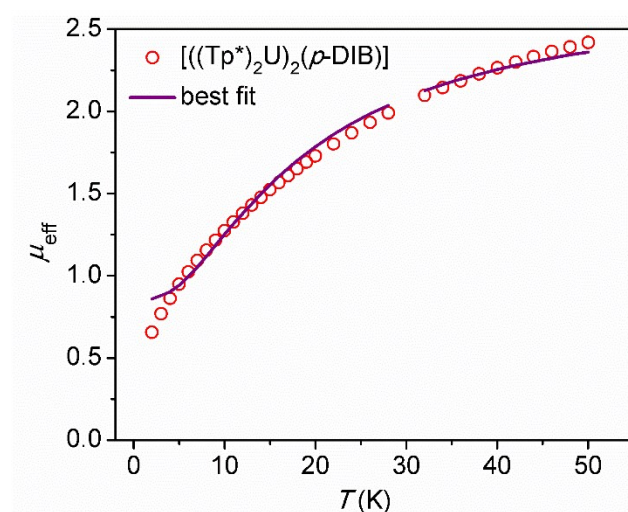


Figure S30. Temperature dependence of the magnetic susceptibility for $[(\text{Tp}^*_2\text{U})_2\text{-}p\text{-DIB}]$ collected at 1000 Oe with associated PHI fit. Note: susceptibility is shown per U ion.

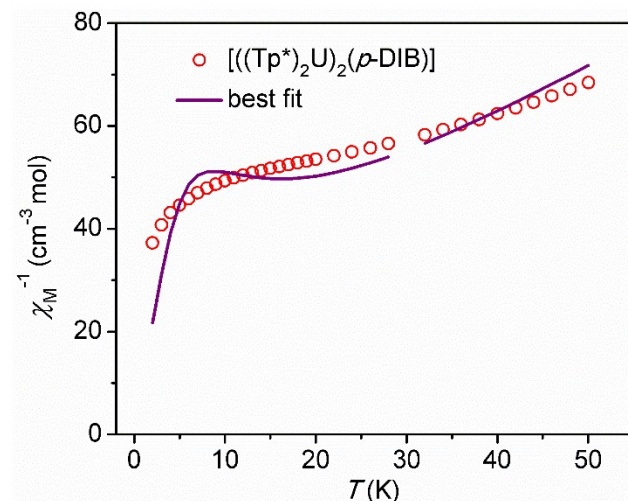


Figure S31. Inverse temperature dependence of the magnetic susceptibility for $[(\text{Tp}^*_2\text{U})_2\text{-}p\text{-DIB}]$ collected at 1000 Oe with associated PHI fit. Note: susceptibility is shown per U ion.

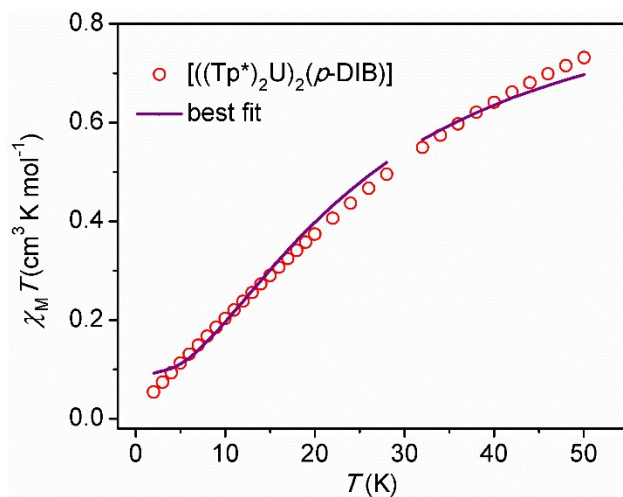


Figure S32. Temperature dependence of the magnetic susceptibility for $[(\text{Tp}^*)_2\text{U})_2\text{-p-DIB}]$ collected at 1000 Oe with associated PHI fit. Note: susceptibility is shown per U ion.

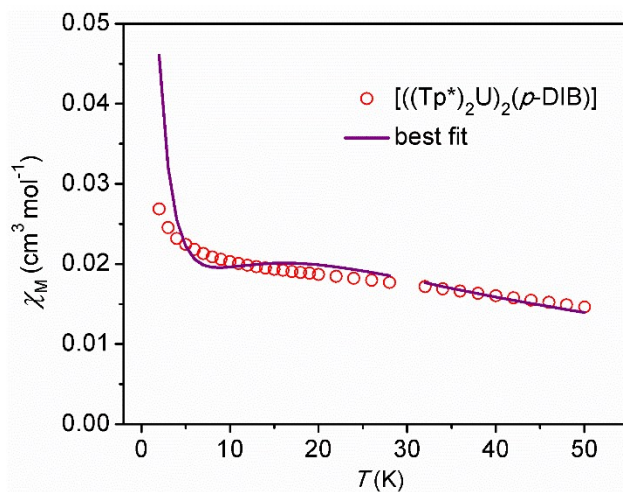


Figure S33. Temperature dependence of the magnetic susceptibility for $[(\text{Tp}^*)_2\text{U})_2\text{-p-DIB}]$ collected at 1000 Oe with associated PHI fit. Note: susceptibility is shown per U ion.

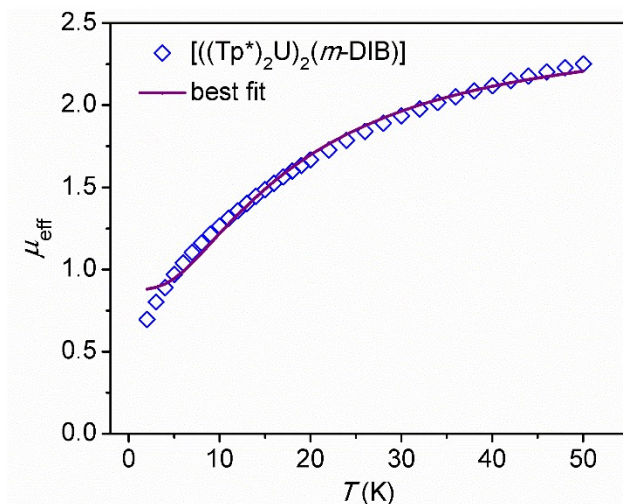


Figure S34. Temperature dependence of the magnetic susceptibility for $[(\text{Tp}^*\text{U})_2\text{-}m\text{-DIB}]$ collected at 1000 Oe with associated PHI fit. Note: susceptibility is shown per U ion.

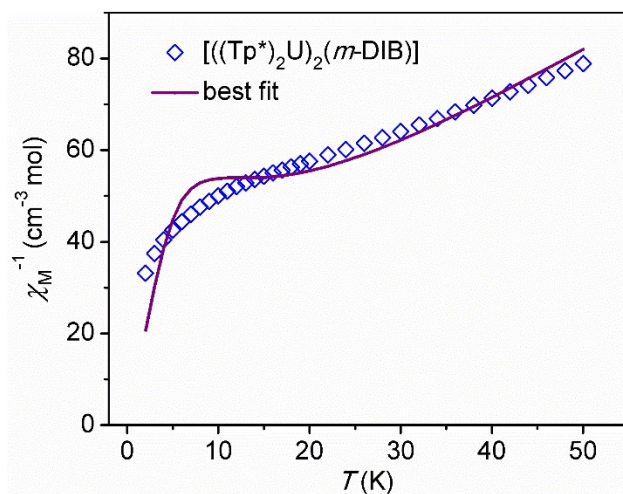


Figure S35. Inverse temperature dependence of the magnetic susceptibility for $[(\text{Tp}^*\text{U})_2\text{-}m\text{-DIB}]$ collected at 1000 Oe with associated PHI fit. Note: susceptibility is shown per U ion.

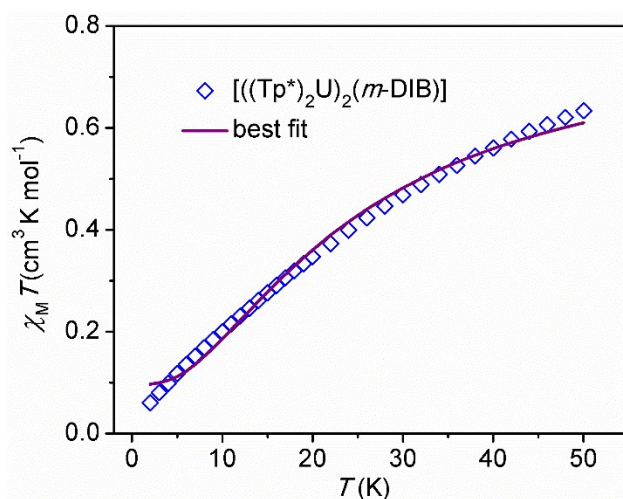


Figure S36. Temperature dependence of the magnetic susceptibility for $[(\text{Tp}^*\text{U})_2\text{-}m\text{-DIB}]$ collected at 1000 Oe with associated PHI fit. Note: susceptibility is shown per U ion.

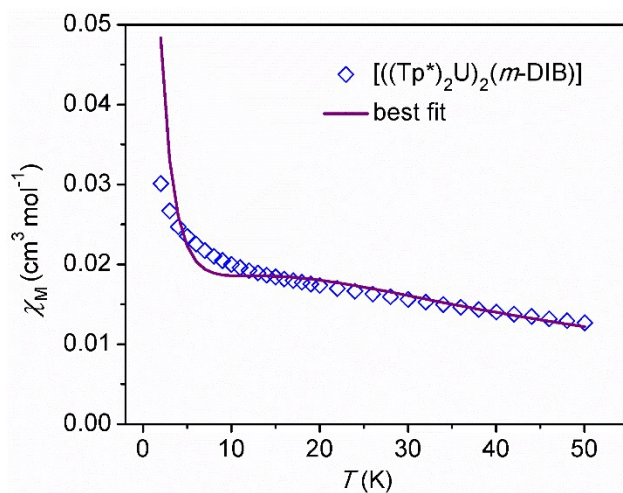


Figure S37. Temperature dependence of the magnetic susceptibility for $[(\text{Tp}^*_2\text{U})_2\text{-}m\text{-DIB}]$ collected at 1000 Oe with associated PHI fit. Note: susceptibility is shown per U ion.

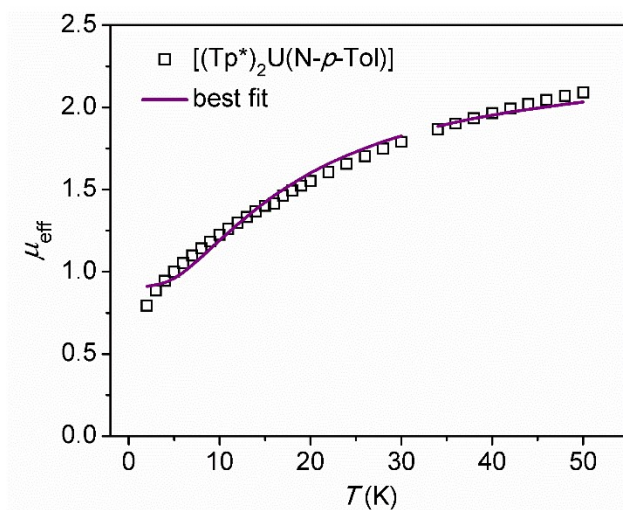


Figure S38. Temperature dependence of the magnetic susceptibility for $[\text{Tp}^*_2\text{U}=\text{N-}p\text{-Tol}]$ collected at 5000 Oe with associated PHI fit.

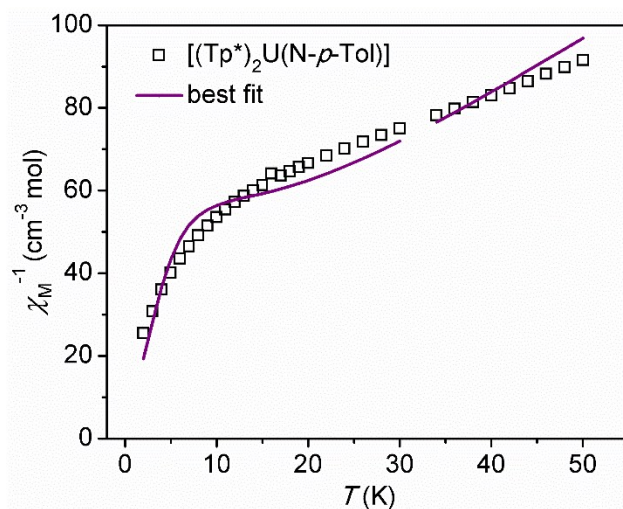


Figure S39. Inverse temperature dependence of the magnetic susceptibility for $[\text{Tp}^*_2\text{U}=\text{N}-p\text{-Tol}]$ collected at 5000 Oe with associated PHI fit.

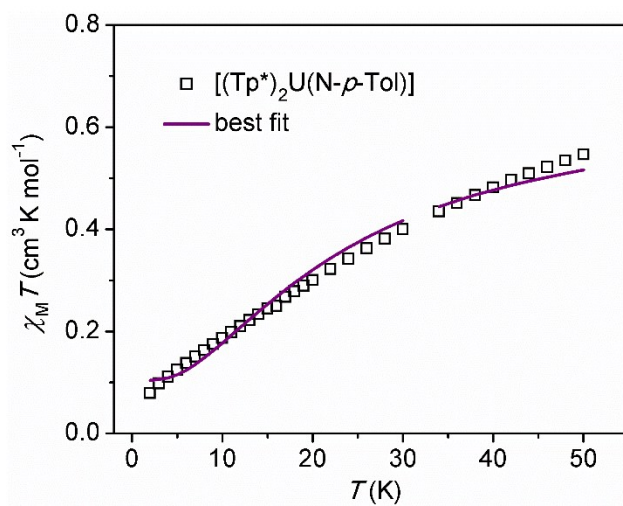


Figure S40. Temperature dependence of the magnetic susceptibility for $[\text{Tp}^*_2\text{U}=\text{N}-p\text{-Tol}]$ collected at 5000 Oe with associated PHI fit.

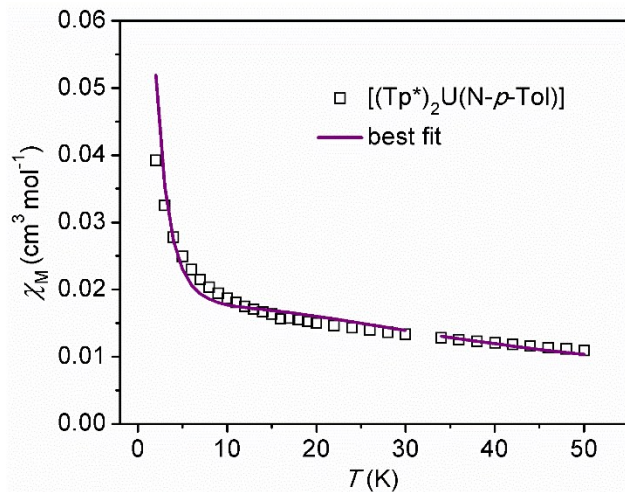


Figure S41. Temperature dependence of the magnetic susceptibility for $[\text{Tp}^*_2\text{U}=\text{N}-p\text{-Tol}]$ collected at 5000 Oe with associated PHI fit.

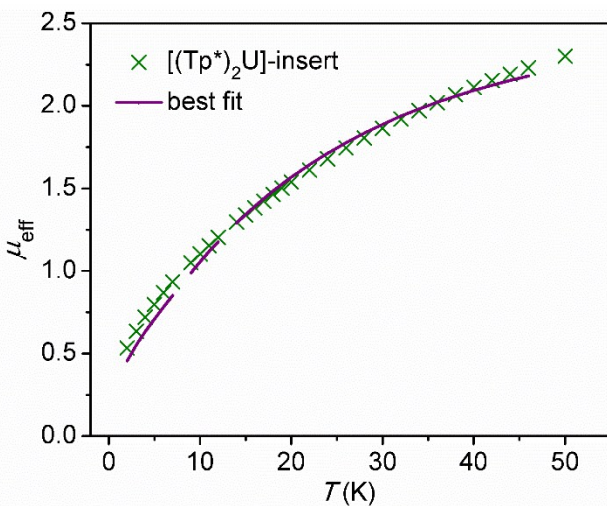


Figure S42. Temperature dependence of the magnetic susceptibility for $[\text{Tp}^*_2\text{U}]\text{-amidinate}$ collected at 1000 Oe with associated PHI fit.

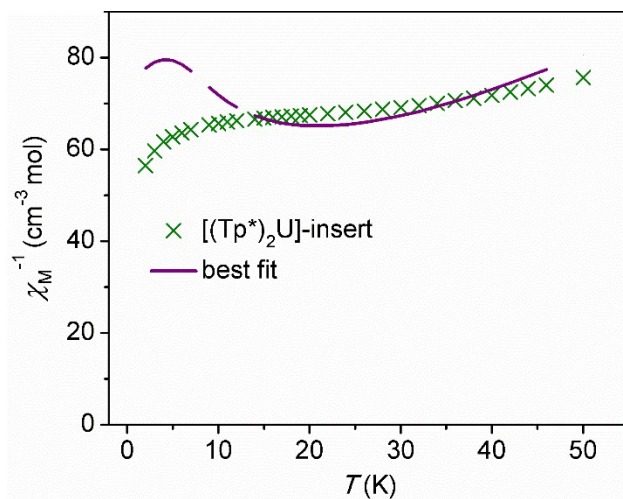


Figure S43. Inverse temperature dependence of the magnetic susceptibility for $[(Tp^*)_2U]$ -amidinate collected at 1000 Oe with associated PHI fit.

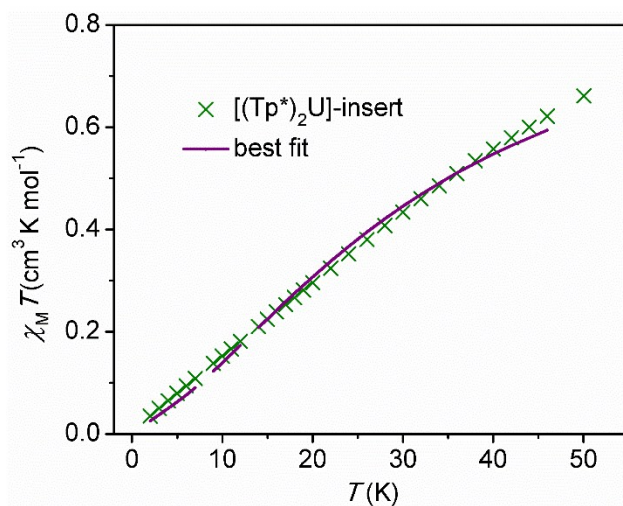


Figure S44. Temperature dependence of the magnetic susceptibility for $[(Tp^*)_2U]$ -amidinate collected at 1000 Oe with associated PHI fit.

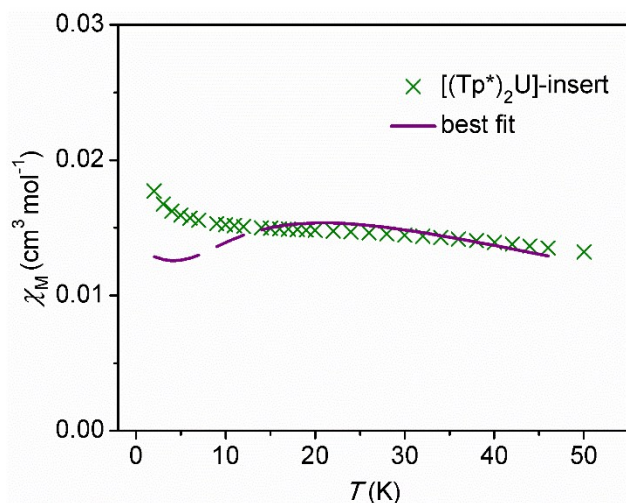


Figure S45. Temperature dependence of the magnetic susceptibility for $[\text{Tp}^*_2\text{U}]$ -amidinate collected at 1000 Oe with associated PHI fit.

Table S1. Selected crystallographic parameters for $\text{U}(\text{Tp}^*)$ complexes.

Complex	Average U-N distance (Å)	U-N range (Å)	$\text{U}\cdots\text{B}$ distance (Å)
$[\text{Tp}^*_2\text{U}=\text{N}-p\text{-Tol}]$	2.64(1)	2.53(1) – 2.786(9)	3.70(1)
$[(\text{Tp}^*_2\text{U})_2-p\text{-DIB}]^a$	2.626(9)	2.508(8) – 2.753(8)	3.69(1)
$[(\text{Tp}^*_2\text{U})_2-m\text{-DIB}]^b$	2.628(9)	2.532(7) – 2.758(7)	3.67(1)
$[\text{Tp}^*_2\text{U}]$ -amidinate	2.610(7)	2.511(5) – 2.775(6)	3.63(1)

^aDue to crystallographic symmetry, only two $\text{U}\cdots\text{B}$ distances are observed, which are 3.69(1) and 3.70(1) (Å). ^bThe four distinct $\text{U}\cdots\text{B}$ distances in the crystal structure are 3.64(1), 3.65(1), 3.67(1) and 3.69(1) (Å). Atom U1 includes the shortest and longest $\text{U}\cdots\text{B}$ distances and U2 includes the other two values.

Table S2. Comparison of different magnetic and crystallographic properties of $\text{U}(\text{Tp}^*)$ complexes.

Complex	τ_0 (1×10^{-6} s)	U_{eff} (cm^{-1})	Closest $\text{U}\cdots\text{U}$ distance (Å)	Average $\text{U}\cdots\text{B}$ distance (Å)	ref
$[\text{Tp}^*_2\text{U}(\text{I})]$	0.18	21.0	9.074(5)	3.478(8)	6
$[\text{Tp}^*_2\text{U}(\text{bpy})](\text{I})$	0.14	18.2	9.455(4)	3.565(8)	5
$[(\text{Tp}^*_2\text{U})_2-p\text{-DEB}]$	--	--	9.064(4)	3.646(3)	this work
$[(\text{Tp}^*_2\text{U})_2-m\text{-DEB}]^b$	--	--	9.9665(6)	3.60(1)	this work
$[\text{Tp}^*_2\text{UCCPh}]$	2.08	6.81	9.983(8)	3.626(8)	this work
$[\text{Tp}^*_2\text{U}(\text{THF})](\text{BPh}_4)$	4.28	9.00	8.893(6)	3.575(6)	this work
$[\text{Tp}^*_2\text{U}(\text{MeCN})_2](\text{BPh}_4)$	4.00	8.36	10.636(7)	3.652(8)	this work

^aIntramolecular $\text{U}\cdots\text{U}$ distance is 13.245 Å. ^bIntramolecular $\text{U}\cdots\text{U}$ distance is 10.743(7) Å.

References

- C. J. Tatebe, J. J. Kiernicki, R. F. Higgins, R. J. Ward, S. N. Natoli, J. Langford, C. L. Clark, M. Zeller, P. Wenthold, M. P. Shores, J. R. Walensky, S. C. Bart, *Organometallics* 2019, **38**, 1031-1040.
- C. J. Tatebe, T. S. Collins, G. R. Barnett, M. Zeller, S. C. Bart, *Polyhedron* 2019, **158**, 1-7.
- G. A. Bain, J. F. Berry, *J. Chem. Educ.* 2008, **85**, 532-536.
- N. F. Chilton, R. P. Anderson, L. D. Turner, A. Soncini, K. Murray, *J. Comput. Chem.* 2013, **34**, 1164-1175.
- M. A. Antunes, L. C. J. Pereira, I. C. Santos, M. Mazzanti, J. Marçalo, M. Almeida, *Inorg. Chem.* 2011, **50**, 9915-9917.

6. J. T. Coutinho, M. A. Antunes, L. C. J. Pereira, H. Bolvin, J. Marçalo, M. Mazzanti, M. Almeida, *Dalton Trans.* 2012, **41**, 13568-13571.
7. J. D. Rinehart, K. R. Meihaus, J. R. Long, *J. Am. Chem. Soc.* 2010, **132**, 7572-7573.